Journal of Fluorescence
https://doi.org/10.1007/s10895-020-02595-y

ORIGINAL ARTICLE

Substantial Cellular Penetration of Fluorescent Imidazoquinoxalines

Cindy Patinote[1] · Natalina Cirnat[1] · Kamel Hadj-Kaddour[1] · Pierre Cuq[1] · Pierre-Antoine Bonnet[1] · Carine Deleuze-Masquéfa[1]

Received: 15 June 2020 / Accepted: 27 July 2020

Abstract
Fluorescent tools have revolutionized our capability to visualize, probe, study, and understand the biological cellular properties, processes and dynamics, enabling researchers to improve their knowledge for example in cancer field. In this paper, we use the peculiar properties of our Imiqualines derivatives to study their cellular penetration and distribution in a human melanoma cell line A375 using confocal microscopy. Preliminary results on colocalization with the potent protein target c-Kit of our lead are also described.

Keywords Imidazo[1,2-*a*]quinoxaline · Fluorescence · Localization · Confocal microscopy · Melanoma · A375 cells.

Introduction

Melanoma is the most dangerous skin cancer, due to its ability to spread throughout the body by metastases. It is thus responsible for 9 deaths out of 10 linked to skin cancers. Diagnosed and treated in the early stages, it can be cured in 90% of cases. Protein kinase inhibitors are used to treat melanomas with a BRAFV600 mutation: vemurafenib, dabrafenib, trametinib and cobimetinib. However, some patients develop resistance mechanisms. These molecular mechanisms varied but mainly lead to reactivation of the MAPK pathway and/or activation of the PI3K-AKT parallel signaling. On the other hand, immunotherapy is reserved for BRAF-negative metastatic patients or mutated BRAF patients who have become resistant. Patients responding to immunotherapy with monoclonal antibodies (nivolumab, ipilimumab, pembrolizumab) cannot be anticipated, and these treatments are extremely expensive. As not all melanomas respond to these therapies, the development of new active treatments against melanoma is a public health concern in view of their ever increasing prevalence.

In this context, we developed original imidazoquinoxalines series, analogues of the Imiquimod parent compound (an immunomodulator marketed in cream under the name ALDARA® effective on certain skin and urogenital cancers such as basal cell carcinoma). From our first generation active Imiqualines published and protected by international patents [1–6], the chemical modulations carried out led to obtaining the second generation [7–10], the leader of which is EAPB02303, protected by a selection patent with international extension [11]. EAPB02303 presents an interesting and selective profile of nanomolar cytotoxic activities on a panel of human cancer cell lines. On our human melanoma cell line A375 reference, the measured activities are superior to those of vemurafenib [9]. Moreover, transcriptomic studies allowed us to show that EAPB02303 displays an original mechanism of action, completely independent of tubulin and different from those of a panel of anticancer agents used in clinics (alkylating agents, topoisomerase inhibitors, anti-metabolites, anti-tubulin). The first *in vivo* results on A375 melanoma xenografted in mice show a higher efficacy of EAPB02303 compared to the reference docetaxel, in the absence of anti-angiogenic or necrotic activity, a low mitotic index and limited toxicity (unpublished results). In this context, EAPB02303 has been determined of particularly great value as a new highly active and selective agent for melanoma treatment [11]. The determination of its extra- or intracellular molecular pharmacological targets is crucial for its successful development toward clinical steps. Actually, it is essential for further development to determine if EAPB02303 primarily binds to the cellular membrane or acts further to internalization within the melanoma cell.

Cindy Patinote and Natalina Cirnat contribute equally to this work.

✉ Cindy Patinote
cindy.patinote@umontpellier.fr

[1] IBMM, Université de Montpellier, CNRS, ENSCM, Montpellier, France

Published online: 10 August 2020

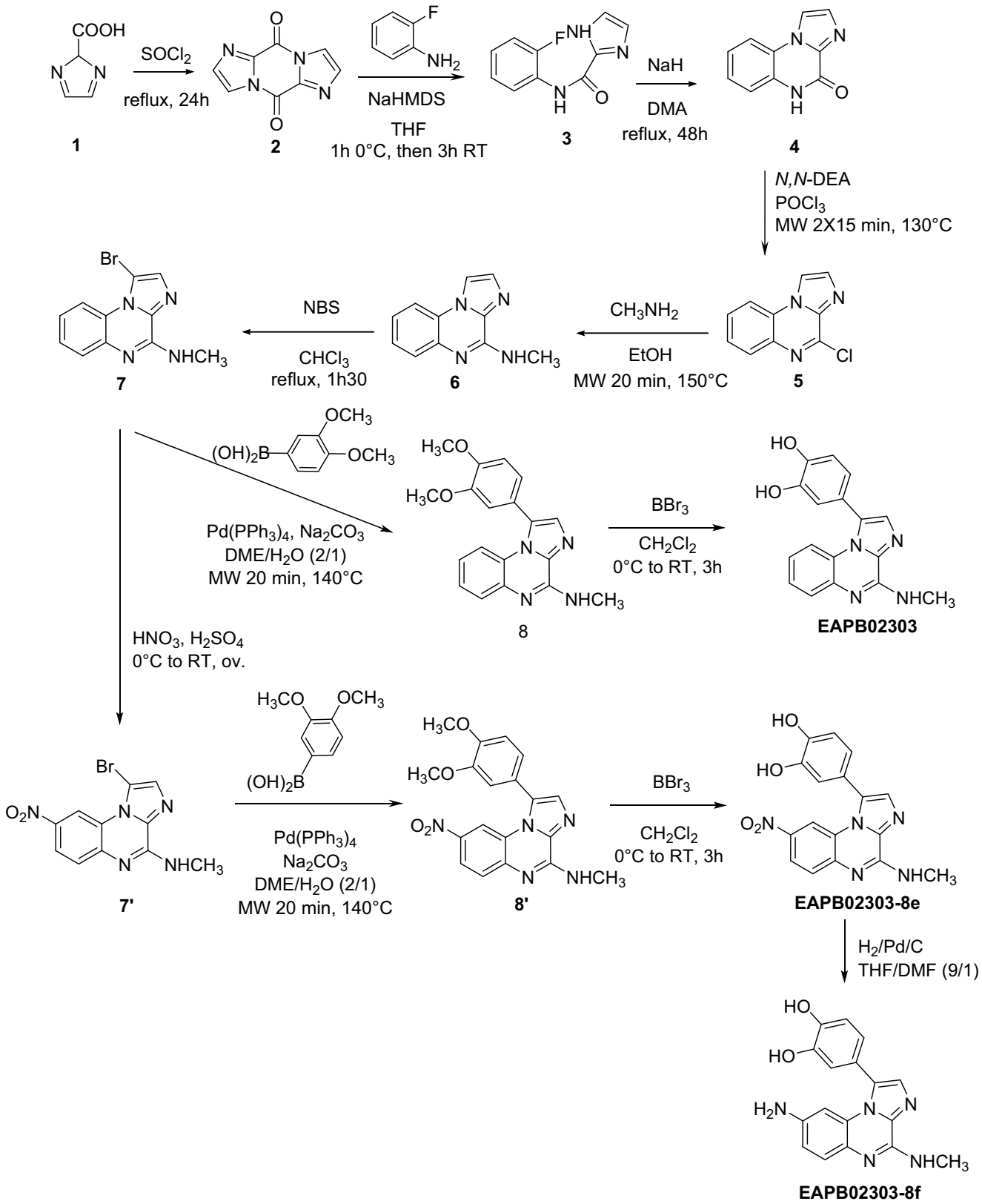

Scheme 1 Synthetic pathways of EPB02303, EAPB02303-8e or EAPB02303-8 f

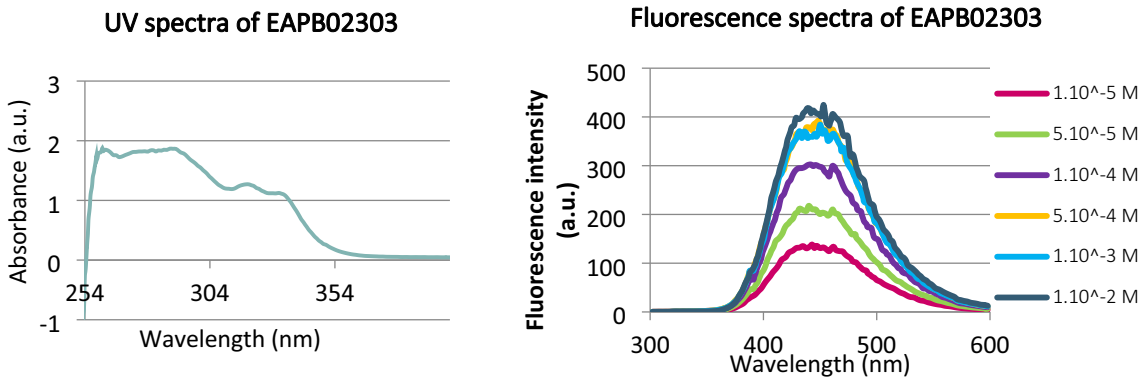

Fig. 1 UV and fluorescence spectra of EAPB02303 in DMSO[22]

In vitro fluorescent imaging (FI) studies enable the detection of drug-protein interactions, protein-protein interactions, gene expression and cellular processes, such as drug internalization and distribution [12–15]. The possibility of studying molecular processes in detail thanks to FI generates information related to cancer progression, as protease activity, apoptosis, necrosis and autophagy [16, 17]. The intrinsic fluorescence of some active compounds could be used to overcome the introduction of fluorescent markers which could modify their biological activity. In fact, unsaturated systems confer fluorescent properties on heterocyclic compounds, which are consequently useful materials for imaging. For example, autofluorescence of anticancer drugs, as doxorubicin and ellipticine, allows for real-time localization, accumulation, time-/dose-dependent cell death studies [18, 19].

Thanks to their planar rigid π-conjugation systems, the parent drug Imiquimod [20, 21] and our Imiqualines derivatives[22] behave as fluorescent chromophores. We previously recorded, analyzed and published in this journal the unpredicted fluorescent properties of some of our eleven imidazo[1,2-*a*]quinoxaline derivatives. Differences were observed concerning their absorbance and emission spectra despite belonging to the same chemical family, notably for the intensities. No auto-quenching fluorescence was detected in the tested experimental conditions. In parallel of ongoing chemical biology studies using affinity chromatography coupled with the SILAC method and associated with high performance mass spectroscopy to confirm specific binding with protein target(s), we investigate in this study the cellular penetration of **EAPB02303** and its localization into human melanoma cells (A375) by using confocal microscopy. In order to gather information and elucidate the mechanism of action of our lead, we present herein first the *in vitro* results obtained with **EAPB02303**, and secondly a detailed localization study of **EAPB02303-8f**, a more suitable derivative for fluorescence imaging. Co-localization with the potent target c-Kit of our drug was also considered.

Materials and Methods

Chemical Compounds and Prepared Solutions

EPB02303, **EAPB02303-8e** and **EAPB02303-8f** synthetic pathways are depicted in Scheme 1. Compounds were synthesized thanks to a route we previously described [11, 13, 16]. Briefly, the carbonylimidazole dimer **2** results from the condensation of the 2-imidazole carboxylic acid **1** in the presence of thionyl chloride. Addition of the *o*-fluoroaniline on the dimer **2** gives the intermediate **3**. Cyclisation is allowed by using sodium hydroxide in dimethylacetamide. Treatment of compound **4** with phosphorus oxychloride and *N,N*-diethylaniline gives the chlorinated compound **5**. Then, an amino group substitutes the chlorine. To obtain the $NHCH_3$ residue **6**, methylamine in ethanol is grafted under microwave assistance. The bromination of the intermediate **6** by *N*-bromosuccinimide led to compound **7**. An additional step to introduce the nitro group on position 8 is carried out with nitric acid in acidic conditions and furnishes compound **7'**. Appropriate aryl boronic acid is introduced in position 1 *via* a Suzuki-Miyaura cross-coupling reactions leading to compounds **8** and **8'**. Intermediates were submitted to boron tribromide to give the hydroxylated derivatives **EAPB02303** and **EAPB02303-8e**. Hydrogenation on Pd/C gives final compound **EAPB02303-8 f.**

Compounds were stored at 4 °C. Stock solutions at 1.10^{-2} m of each compound were prepared in DMSO. These working standard solutions were then diluted with DMSO or Dulbecco's Modified Eagle's Medium (DMEM) to obtain 1.10^{-9} m to 1.10^{-4} m as final concentrations for studies described below.

Absorption and Fluorescence Spectra

Absorption spectra were recorded on an UV-visible spectrophotometer (Cary 400, Varian) from 250 to 400 nm. Fluorescence spectra were recorded on a fluorescence spectrophotometer (Cary Eclipse, Varian) from 300 to 600 nm.

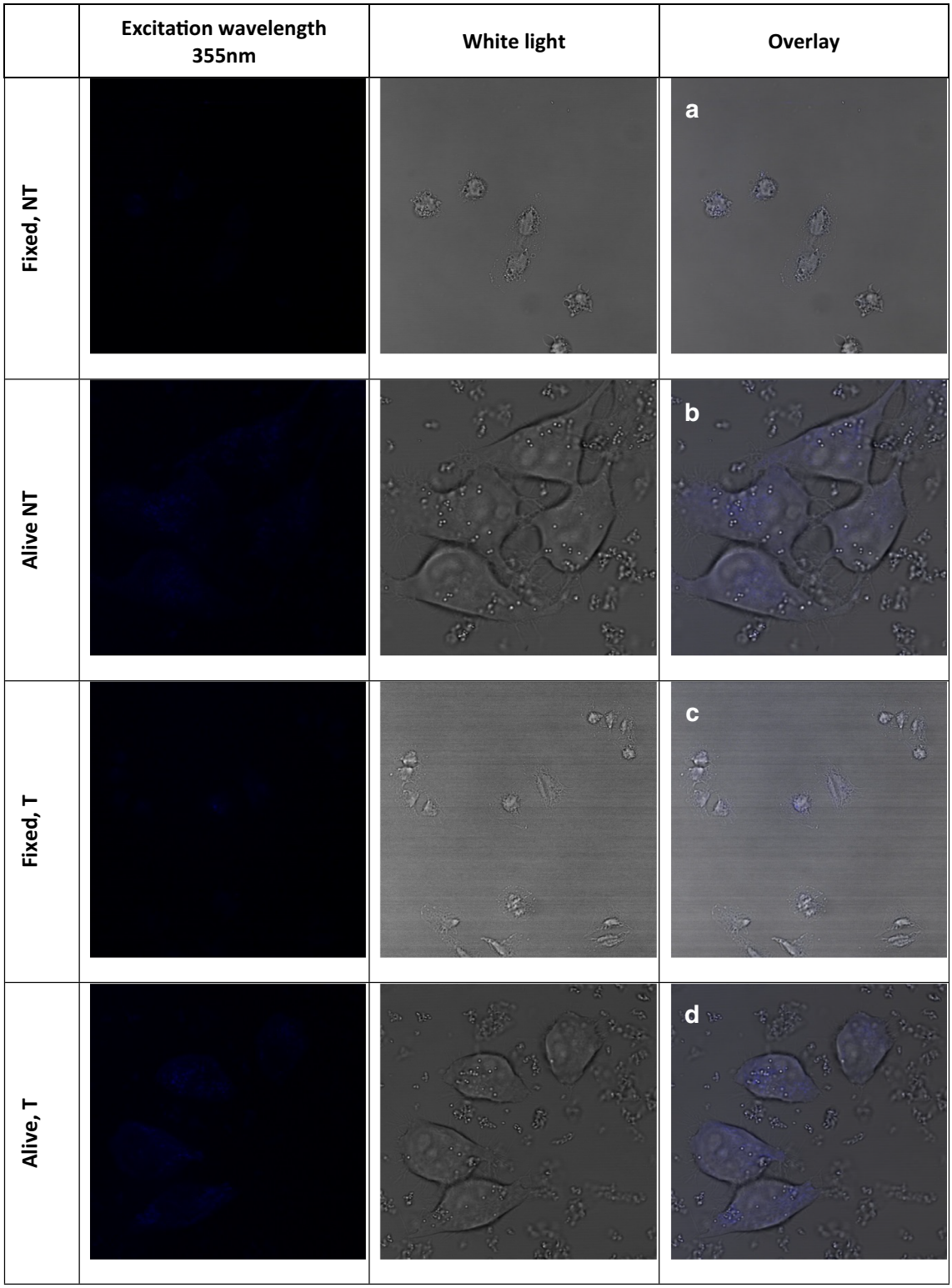

Fig. 2 Images from fluorescence microscopy experiments with fixed or non-fixed A375 cells incubated (T) or not (NT) for 1 h at 37 °C in medium containing 3 nM of EAPB02303. The third column represents the overlay of direct fluorescence output (blue, first column) and white-light reflectance (second column)

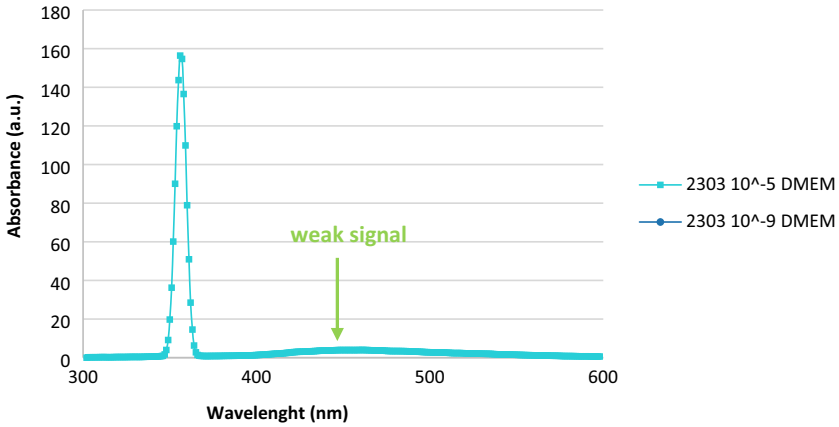

Fig. 3 UV spectra of EAPB02303 recorded with the same used *in vitro* conditions

Cell Culture

The A375 human melanoma cell line were grown in DMEM supplemented with 10% fetal calf serum, 1% glutamine and antibiotics and incubated at 37 °C in an atmosphere of 5% CO_2 in air. Cells were grown as attached monolayer and were detached for experiments using short exposure to trypsin. Cell concentrations were determined using a CASYton® counter.

Confocal Laser Scanning Microscopy

The confocal imaging system used was Multiphoton Microscope Leica™ TCS SP8 equipped with a 355 nm laser and a 63x objective (1.4 NA). Cells were grown at a density of 5.10^4 cells/well as a monolayer on autoclaved glass Fluorodish® or 8-well tissue culture chambers (Sarstedt™) at the time of drug exposure. Cells were treated with **EPB02303**, **EAPB02303-8e** or **EAPB02303-8f** during various incubation times. The cells were fixed with 4% PFA and examined under the confocal laser scanning microscope (Leica Microsystems™).

Cell Fluorescence Measuring

The level of cellular fluorescence from fluorescence microscopy images was determined using ImageJ. The corrected total cell fluorescence (CTCF) was calculated by the formula:

$$\text{CTCF} = \text{Integrated Density} - (\text{Area of selected cell}) \times (\text{Mean fluorescence of background readings}).$$

Results and Discussion

The efficacy of a drug relies upon one or more interaction(s) with a relevant target protein implicated in the pathological process. The detection and the characterization of the binding of our lead to its intended target remain a scientific challenge [23]. In order to specify not only the mechanism of action but also the targeted protein(s) of our lead EAPB02303 and its analogues implicated in the treatment management of melanoma

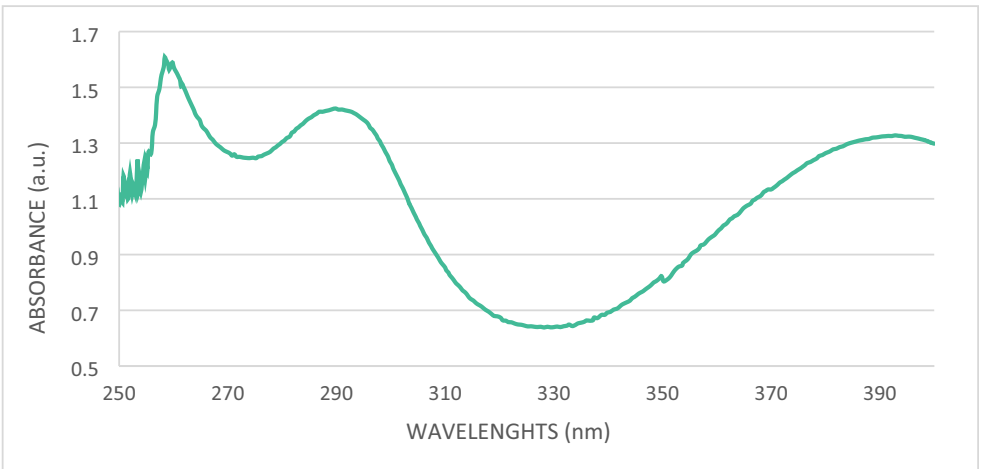

Fig. 4 UV spectrum of EAPB02303-8e

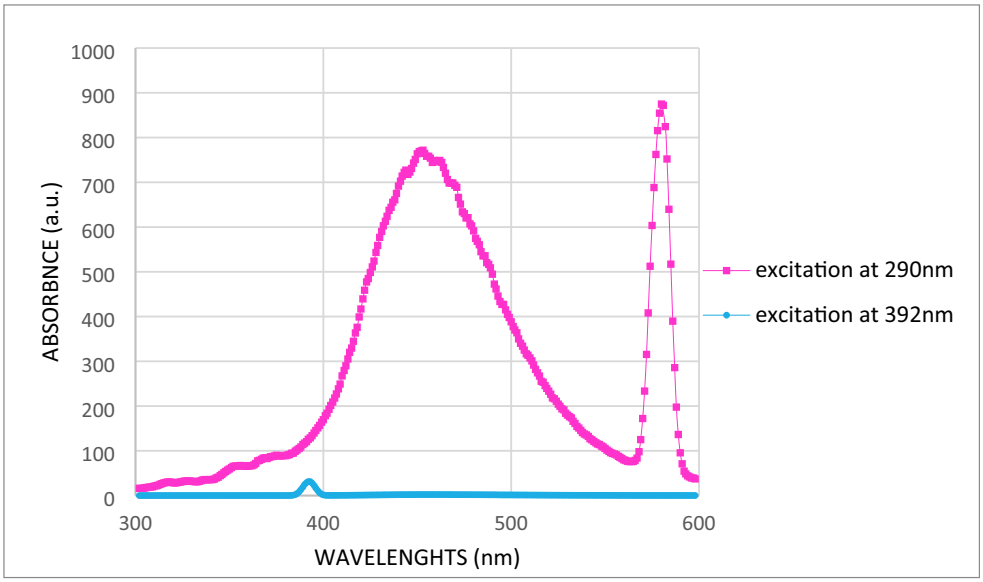

Fig. 5 Fluorescence spectra of EAPB02303-8e

disease, we decided to use the fluorescent properties of our compounds to obtain keys for elucidating them. We first investigated the localization, distribution and accumulation of **EAPB02303** and **EAPB02303-8f**, the most suitable agent for confocal microscopy imaging. Even if fluorescence is often criticized due to numerous artifacts (ionic strength, solvent polarity, pH, temperature, natural fluorescence of the cells) which parasitize the signal emitted by the imaging agents, we described herein promising results for our compound **EAPB02303-8 f.** Furthermore, preliminary tests were performed here to evaluate cKit as potent target protein, as cKit was the only highlighted protein among a panel of screened kinases (data not shown). Moreover, markers of colocalization of the nucleus and mitochondria were also used secondly to examine more precisely the distribution of the compound **EAPB02303-8 f.**

Preliminary Studies

Absorption Spectra of EAPB02303 in DMSO

The UV profile and fluorescent spectra of **EAPB02303** in DMSO were previously published [22]. Our paper showed that UV spectra are in concordance with the presence of the catechol moiety on the one hand and with the quinoxaline core on the other hand (Fig. 1). Moreover, there is a quantifiable fluorescent response with a maximum at 445 nm when excited at 270 nm at a concentration of 1.10^{-4} m.

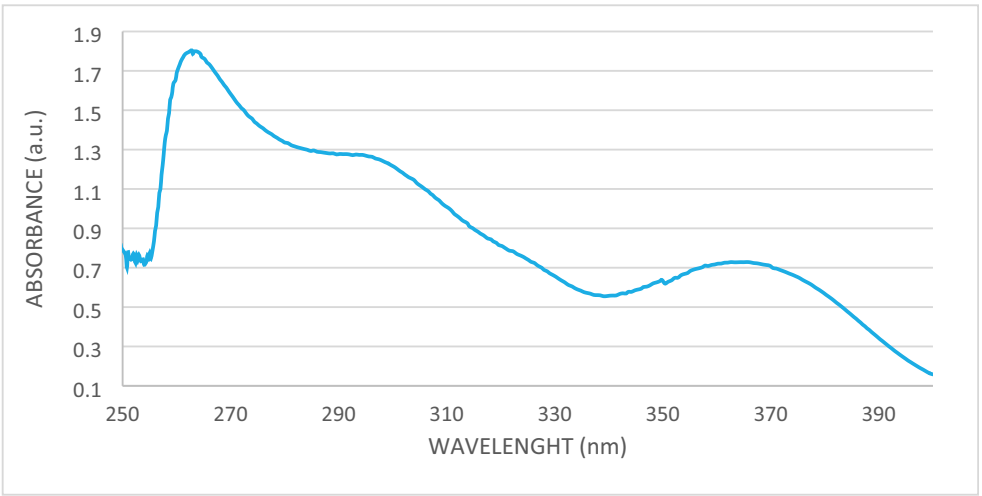

Fig. 6 UV spectrum of EAPB02303-8f in used conditions

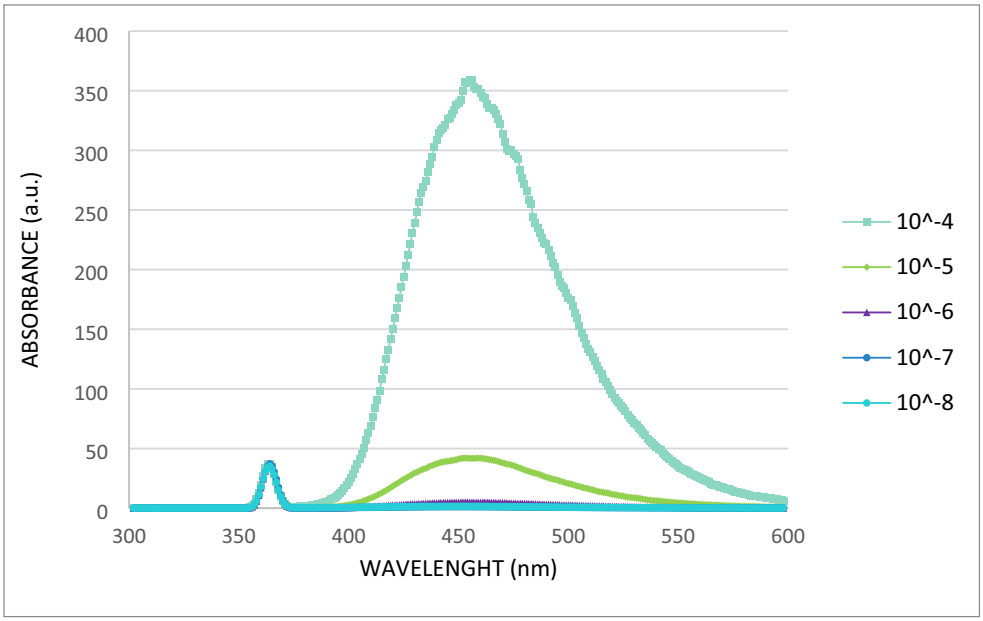

Fig. 7 Fluorescence spectra of EAPB02303-8f in DMSO after exciting at 364 nm

Samples for Confocal Laser Scanning Microscopy

The A375 cells were plated about 24 h before the start of the test on the 35 mm diameter glass slides (FluoroDish™) containing 1.5 mL of DMEM growth medium without a phenol red pH indicator. The number of cells seeded was adjusted to have about 50,000 / FluoroDish™ at the time of exposure to **EAPB02303**. 1.5 mL of **EAPB02303** at 10^{-9} m was added to previously prepared plated cells and left for 1 h incubation at 37 °C. One FluoroDish™ was used as negative control. After the incubation period, 1 mL of 4% paraformaldehyde (PFA) was added (10 min in the dark, covered with a polystyrene box). PFA was washed three times with 1.5 mL PBS during 2–5 min at RT without shaking.

Confocal Fluorescent Microscopy

Based on the significant fluorescent signal of **EAPB02303**, we started confocal microscopy studies in the aim of determining the cell penetration of the compound. For the first confocal imaging analysis, we diluted **EAPB02303** stock solution in DMEM without red phenol buffer until 10^{-9} m as its anticancer activity is in the nanomolar range. Even if UV signal is low above 350 nm, the possibility to obtain a fluorescence signal after excitation at 355 nm is not implausible. To our astonishment, no fluorescence signal was detectable after one hour of incubation time with 3 nM of **EAPB02303** compared to control (Fig. 2, A compared to C, B compared to D). Furthermore, an auto-fluorescence phenomenon of A375

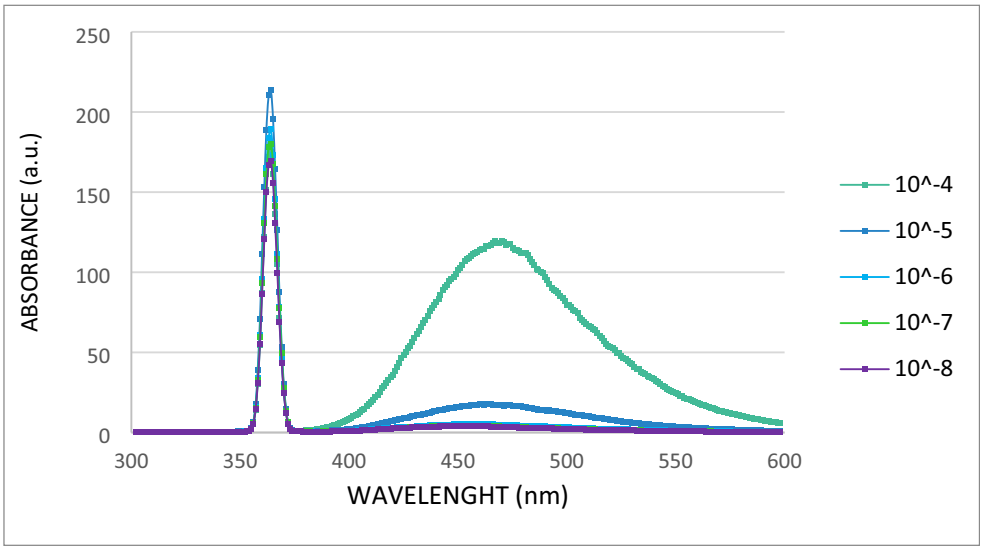

Fig. 8 Fluorescence spectra of EAPB02303-8f in DMEM after exciting at 364 nm

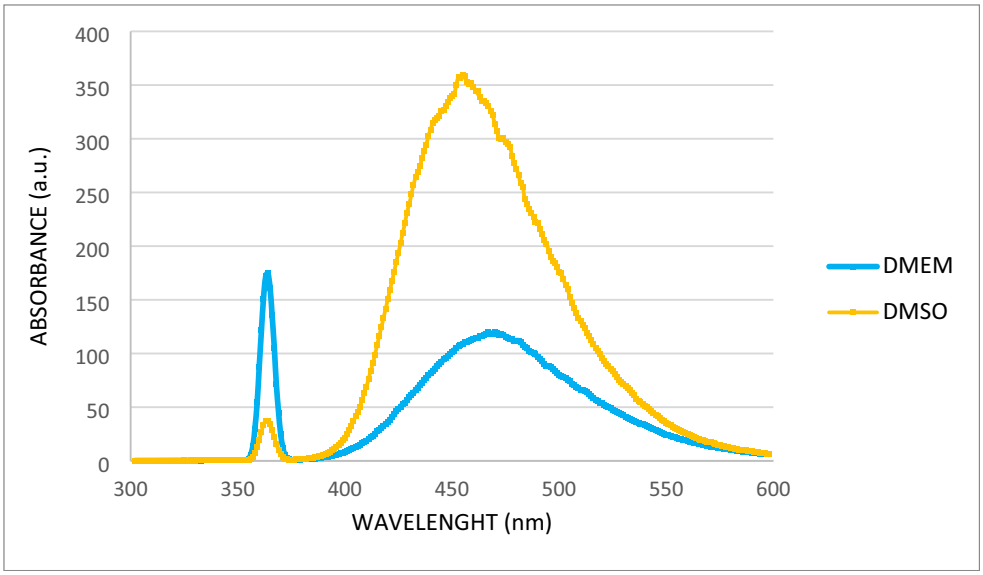

Fig. 9 Superposition of fluorescence spectra of EAPB02303-8f at 10^{-4} m in DMSO and DMEM after exciting at 364 nm

cells has been highlighted. This phenomenon is associated with ABCG2 expression in A375 cell line as demonstrated by Marzagalli et al.. in the same time of our study [24]. Some little round vesicles are also detected (visible as white points in pictures of Fig. 2).

We hypothesized that the DMEM buffer may change or interfere in the fluorescence signal of **EAPB02303**. In fact, the autofluorescence of phenol-red free DMEM buffer is not unknown, inciting manufacturers such as Thermo Fischer to produce lower fluorescent DMEM-containing buffer [25]. In order to eliminate the possibility that DMEM buffer impacts and stops the fluorescent signal of **EAPB02303**, the absorption spectra of the compound needed to be verified in the studied cell environment.

Fluorescence Spectra of EAPB02303 in DMEM Buffer

Solutions of compound **EAPB02303** between 10^{-5} m and 10^{-9} m in phenol-red free DMEM buffer were prepared from the stock solution at 10^{-2} m in DMSO. When excited at 355 nm, no convenient fluorescent signal was recorded, except a very weak signal at 450 nm, which confirms us what we observed *in vitro* (Fig. 3). A thin peak appears at 355 nm corresponding to the recovering emitting light.

In vitro Localization Studies

UV and Fluorescence Spectra of EAPB02303-8e and EAPB02303-8f in DMEM Buffer

As the fluorescent signal of **EAPB02303** was completely lost in the used conditions, we turned our attention to the bank of **EAPB02303** derivatives synthesized in our laboratory. Two interesting compounds, **EAPB02303-8e** and **EAPB02303-8f**, were further analysed for their fluorescence properties since their biological activities are in the same nanomolar range than the leader **EAPB02303** on A375 melanoma cell line. The advantages of **EAPB02303-8e** and **EAPB02303-8f** lie on their electronic rich chemical groups (NO_2 and NH_2) grafted on the heterocycle which are not present in the **EAPB02303** chemical structure. Those chemical groups could confer useful additional fluorescent properties for cellular localization.

UV spectrum of **EAPB02303-8e** is similar to spectra of our quinoxaline family and is depicted in Fig. 4. Data shows two successive waves with maxima around 260 and 292 nm respectively then a decrease until 330 nm before increasing until 400 nm. No absorbance was detected after 400 nm in the visible region.

Considering these results, a 10^{-4} m sample in DMSO is excited at 392 nm. A very low emission response at 461 nm is detected but not sufficient to continue the cellular localization studies with this compound since the excitation range of the confocal laser starts at 355 nm (Fig. 5). Out of curiosity, this sample is excited at 290 nm, which corresponds to a peak on its UV profile (NB: we excited at 270 nm in our previous publication). The fluorescence response is of quality with an emission at 453 nm (intense and wide peak) and at 580 nm (intense and fine peak) (Fig. 5). This result shows that a compound is able to absorb energy (UV profile) at certain wavelengths but unable to necessarily re-emit fluorescence energy.

Fig. 10 Fluorescence microscopy experiments with A375 cells incubated for 15 min, 30 min, 1 and 2 h at 37 °C in medium containing 10^{-5} M of EAPB02303-8 f. Direct fluorescence observed upon irradiation with 355 nm light. The third column represents the overlay of direct fluorescence output (blue, first column) and white-light reflectance (second column)

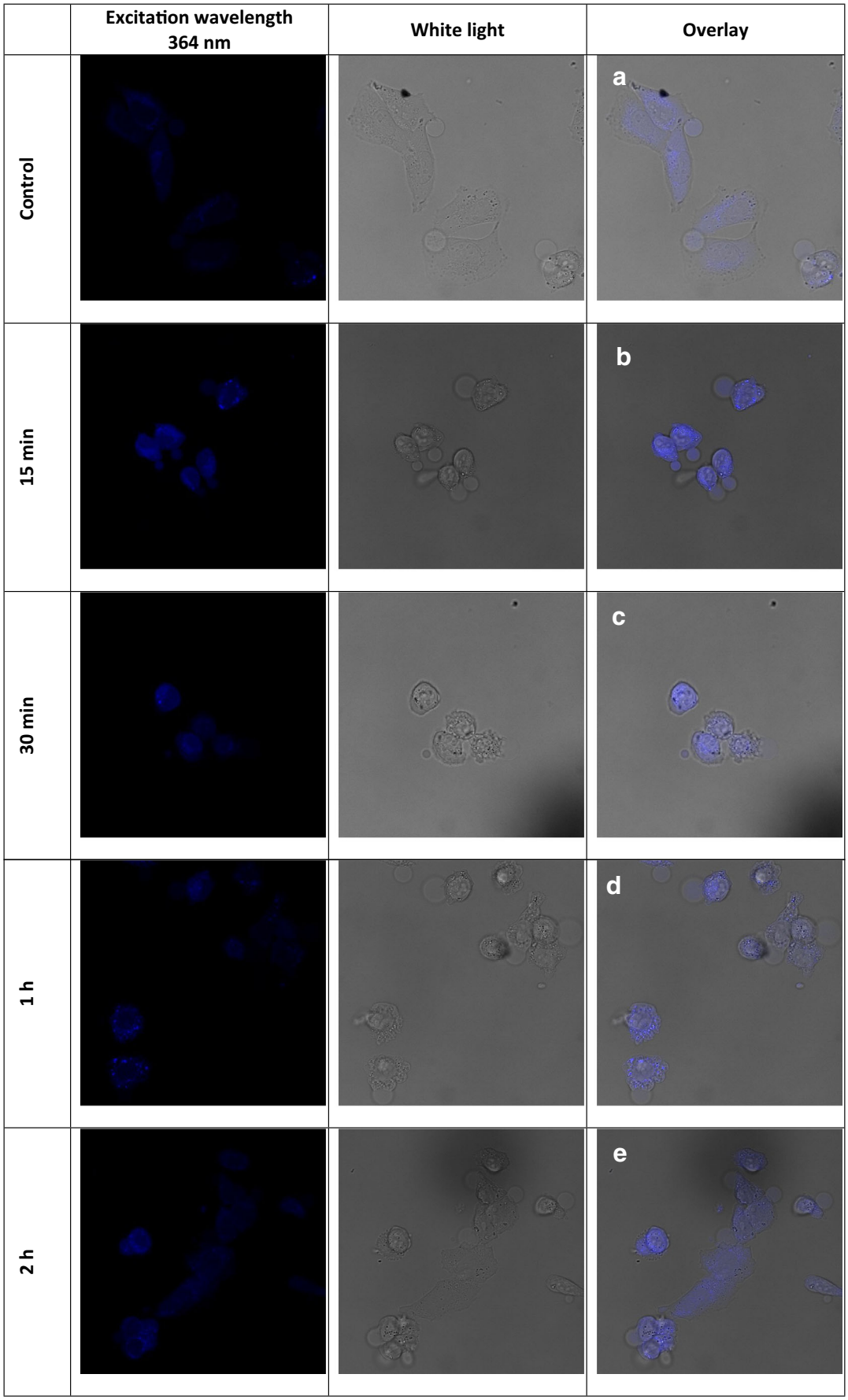
Excitation wavelength 364 nm
White light
Overlay
Control
15 min
30 min
1 h
2 h
a
b
c
d
e

UV spectrum of **EAPB02303-8f** is depicted on Fig. 6. Data show first maximum at 265 nm. The curve is decreasing until a plateau around 296 nm. A secondary lower maximum is observed around 364 nm, and fluorescence is finally lost before 400 nm. A sample at 10^{-4} m in DMSO is first excited at 364 nm. The fluorescence spectrum shows a correct emission at 455 nm. A dilution range of 10^{-5} m, 10^{-6} m, 10^{-7} m, 10^{-8} m in DMSO was prepared and the samples were excited at 364 nm. Below 10^{-6} m, the signal is no longer detectable (Fig. 7). Moreover, a dilution range of 10^{-5} m, 10^{-6} m, 10^{-7} m, 10^{-8} m of **EAPB02303-8f** is prepared in DMEM without phenol red from a 10^{-2} m stock solution of **EAPB02303-8f** in DMSO, and same results are observed: the fluorescent signal is lost only beyond 10^{-6} m (Fig. 8). We could also observe a fine peak corresponding to the recovering emitting light at 355 nm, which is more intense than the fluorescence answer of the compound **EAPB02303-8f** at this excitation rate. The superposition of fluorescence spectra of **EAPB02303-8f** in DMEM and DMSO at 10^{-4} m is depicted on Fig. 9. The fluorescence response obtained by diluting our compound in DMEM buffer is lower than the sample diluted in DMSO at the corresponding concentrations. Thus, it can be deduced that the signal loss during preliminary studies is due firstly to the high dilution used for the incubation and secondly to the presence of the DMEM which must trap a part of or interfere with the emitted energy. For the following results presented herein, we used **EAPB02303-8f** at a 10^{-5} m concentration in DMSO in order to assure a pick-up signal. Moreover, we decided to work on fixed cells which allow a DMEM free medium for imaging recording.

Samples for Confocal Laser Scanning Microscopy

The A375 cells were plated about 24 h before starting the test on 35 mm diameter glass slides (FluoroDish™) containing 1.5 mL of phenol-red free DMEM growth medium. The number of seeded cells was adjusted to have about 50,000 cells/FluoroDish™ for exposure to **EAPB02303-8 f.** 1.5 mL of **EAPB02303-8f** at 10^{-5} m in DMSO was added to previously prepared plated cells and left in incubation at 37 °C for 15 min, 30 min, 1 and 2 h. One FluoroDish™ was used with 1.5 mL of DSMO as negative control. After the respective incubation periods, 1 mL of 4% paraformaldehyde (PFA) was added and left 10 min in the dark (covered with a polystyrene box). PFA was washed three times with 1.5 mL PBS during 2–5 min at RT without shaking.

Results of Confocal Fluorescent Microscopy

The auto-fluorescence observed in non-treated human melanoma cells was clearly detected in an area-dependant way. Fluorescence was primarily observed within cytoplasmic inclusions (such as vesicles) with a general cytoplasmic staining (Fig. 10a). For 15 min incubation (Fig. 10b), fluorescence was apparent but could not be quantified correctly due to quick photobleaching. The photobleaching phenomenon was observed for all incubation periods but stabilized at around 2 h. By this way, to prevent premature light extinction, laser was off while searching cells to be analysed and on when just starting recording data. For 30 min incubation (Fig. 10c), some cells seem suffering, maybe due to the high quantity of **EAPB02303-8 f.** Weak increased fluorescence could be measured after 1 h of exposure (Fig. 10d), and slightly above background noise. Image analysis of cells exposed up to 2 h revealed a 3-fold increase of fluorescence intensity, which is assigned to our compound (Fig. 10e and Table 1). Here again, we noticed fluorescent intracellular vesical, morphologically different from those in control cells which might suggest an endocytic phenomenon additional to the initial passive passage of the cellular membrane.

Co-localization Preliminary Studies

Given the results of the localization study and out of curiosity for these fluorescent vesicles observed in cells, we tried to determine if the target of our compound **EAPB02303-8f** is on the cellular membrane using a plasmatic membrane specific dye on the one hand and an immunofluorescent assay on the other hand. The immunofluorescent assay was designed to determine if **EAPB02303-8f** binds to the cellular receptor c-Kit.

Secondary Immunofluorescence Assay - Colocalization of EAPB02303-8f and c-KIT

Samples for Confocal Laser Scanning Microscopy The A375 cells were plated about 24 h before starting the test on sterile 8-well Tissue Culture Chambers (Sarsted™) containing 0.5 mL of DMEM growth medium. The number of cells seeded was adjusted to have about 10,000/well at the time of exposure to **EAPB02303-8 f.** 0.5 mL of **EAPB02303-8f** at 10^{-5} m in DMSO was added to previously prepared plated cells and left in incubation for 2 h at 37 °C. At least one well was used as negative control. The washing buffer was 1xPBS 0.1% Tween 20 (PBST). Cells were fixed using 4%

Table 1 Corrected total cell fluorescence analyzed by confocal fluorescent microscopy (CTCF mean values).

Incubation times	NT	15 min	30 min	1 h	2 h
CTCF/CTCF NT	1,0	1,3	0,92	1,1	**2,9**
CTCF	237,379	296,842	217,420	259,486	699,184

Images treated with ImageJ., NT = non-treated cells

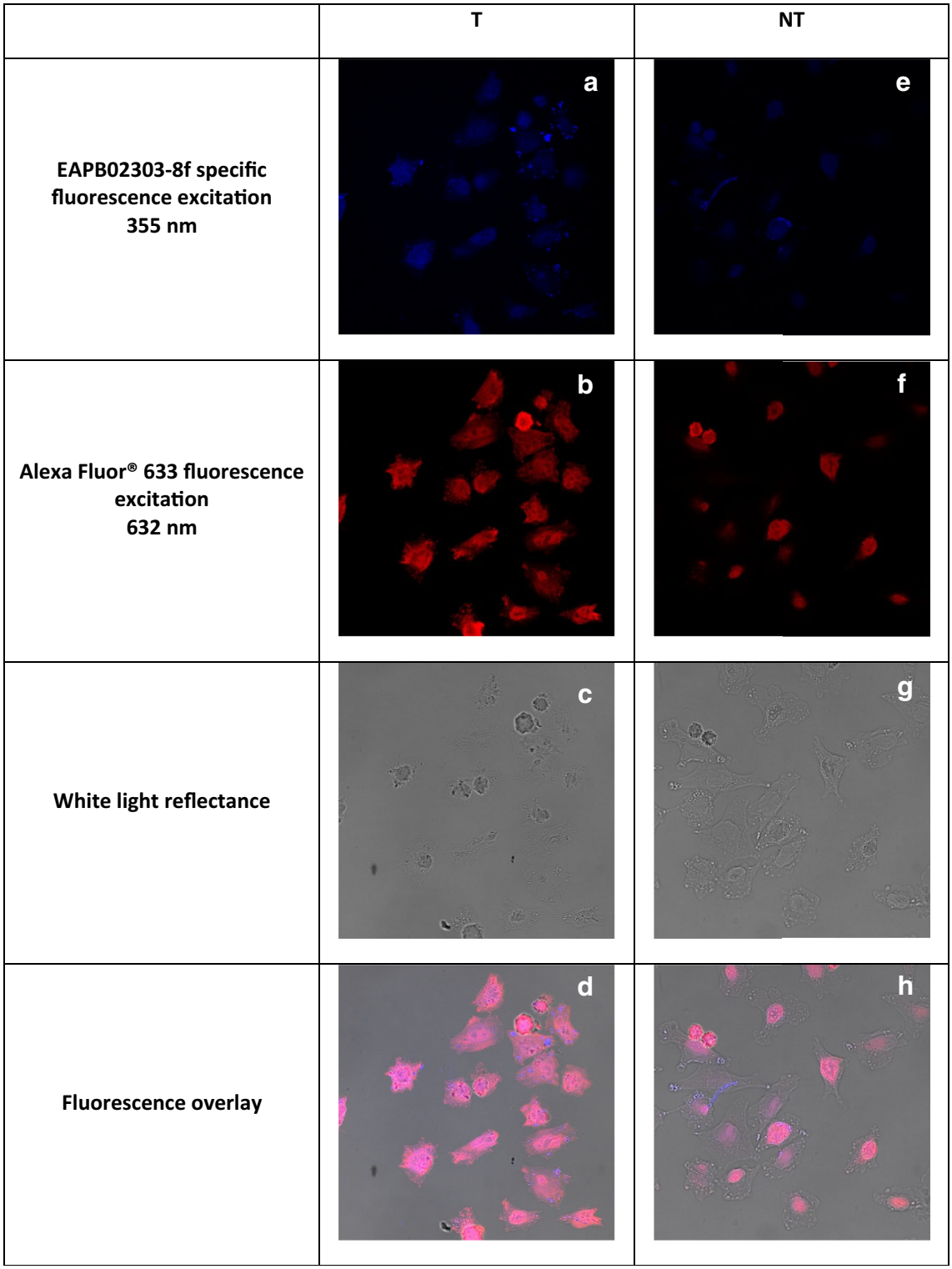

Fig. 11 Images from fluorescence microscopy experiments with A375 cells incubated with the primary antibody and with the secondary antibody. T: A375 cells incubated for 2 h at 37 °C in medium containing 10^{-5} M of EAPB02303-8 f. NT: negative control A375 cells. Direct fluorescence observed upon irradiation with 355 nm light and 632 nm. The forth column represents the overlay of direct fluorescence outputs and white-light reflectance

PFA in PBS, pH 7.4 for 15 min at room temperature. The permeabilization method consisted in 10 min incubation with 0.1% Triton X-100. The cells were then washed by PBS three times. The cells were incubated for 1 h at room temperature with 3% BSA in PBST to block unspecific antibodies binding, and then washed three times in PBST. Cells

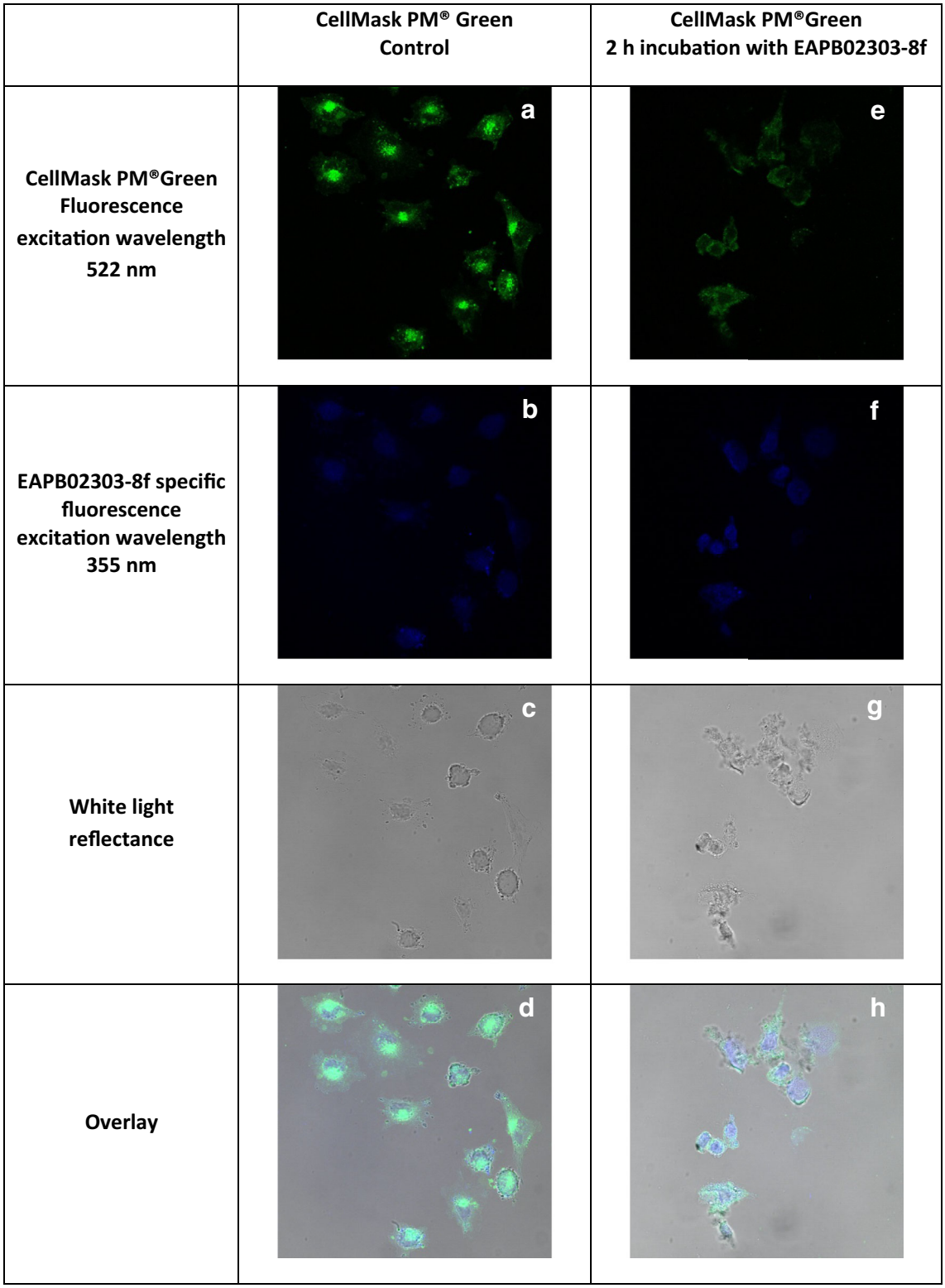

Fig. 12 Images from fluorescence microscopy experiments with A375 cells stained with CellMask® Green PM. T: A375 cells incubated for 2 h at 37 °C in medium containing 10^{-5} M of EAPB02303-8 f. NT: negative control A375 cells. Direct fluorescence observed upon irradiation with 355 nm light and 522 nm. The forth column represents the overlay of direct fluorescence outputs and white-light reflectance

were incubated with the diluted primary antibody (cKIT Antibody, Abgent™) in 3% BSA PBST at room temperature for 1 h. The solution was decanted and then washed three times in PBST. Cells were then incubated with the secondary

antibody in 3% BSA-PBST for 1 h at room temperature in the dark. The secondary antibody solution was decanted and the cells were washed three times in PBST. The coverslips were then mounted with a drop of Fluoroshield® and stored in dark at 4 °C.

Results of Confocal Fluorescent Microscopy Firstly, a difference in fluorescence intensity between the A375 cells treated with **EAPB02303-8f** and untreated is noticed, which is consistent with previous results. We also perceived more vesicles with higher fluorescence intensity in the treated cells (Fig. 11a). The secondary antibody, ALEXA633® seems more internalized and diffuse in the treated cells (Fig. 11a and f). Nevertheless, its strong presence in untreated cells indicates that the non-specific saturation step was not sufficient (Fig. 11a and e). Interestingly, during the superposition of the fluorescence channels, it is noticed that the vesicles corresponding to the fluorescence of **EAPB02303-8f** do not overlap with the fluorescence of the revealing antibody. As a reminder, the incubation time with **EAPB02303-8f** was set at 2 h in agreement with the results of intracellular fluorescence detection. This fluorescence was significantly greater compared to the control cells during a 2 h incubation at a concentration of 10^{-5} m in DMEM. The incubation period with **EAPB02303-8f** of 2 h is probably too long to visualize a binding process or a plasmatic membrane target.

Fluorescence Colocalization Microscopy Analysis Using CellMask® Green Plasmatic Membrane Fluorescent Marker (Invitrogen™)

Samples for Confocal Laser Scanning Microscopy A375 cells were grown on coverslips inside a tissue culture dish with the DMEM medium and incubated with **EAPB02303-8f** following the same procedure as for immunofluorescent experiment. Cells were fixed in 4% PFA solution. The coverslips were quickly submerged in the staining CellMask® Green PM 2X solution (Invitrogen™) for 5 min at 37 °C. The coverslips were rinsed in PBS three times before being mounted and stores at 4 °C.

Results of Confocal Fluorescent Microscopy Figure 12 shows the fluorescence microscopy images of plasmatic membrane stained cells (green). Unexpectedly, the vesicles presumed to be specific of **EAPB02303-8f** are more intense in non-treated cells (Fig. 12a). Likewise, our compound does not appear to be on the plasmatic membrane but is more likely to be diffused in cytoplasm of A375 cells (Fig. 12f). Nevertheless, few cells in both conditions survived the fixation step, so the comparison is not interpretable. Here again, one can imagine that the incubation time with the compound **EAPB02303-8f** is too long to demonstrate membrane colocalization.

Conclusion

The development of new anticancer drugs is a scientific challenge and, presently, fluorescence is used to elucidate part of the mechanism of cancer activity. Thanks to a first study published in this journal, we have highlighted the peculiar fluorescence properties of our Imiqualines. Among different compounds, we identified **EAPB02303-8f** as the best one to study the cellular penetration and localization into melanoma A375 cells. Optimization of visualization conditions were necessary. By this way, we used the compound at a concentration of 10^{-5} m in DMSO for treating cells that have been then fixed for confocal microscopy study, in order to avoid the use and presence of DMEM which induces a loss of fluorescence. We were able to detect correctly our compound **EAPB02303-8f** especially after 2 h of incubation, thanks to a fluorescence 3-times higher than control. Concerning its subcellular distribution, **EAPB02303-8f** is mainly internalized in vesicles, without a specific accumulation in an organelle or nucleus. As we presumed that **EAPB02303-8f**'s target might be a cytoplasmic localized receptor cKIT, we also performed preliminary tests of colocalization in A375 human melanoma cells. This study allows us to obtain interesting information even if **EAPB02303-8f** compound does not correspond to a perfect fluorophore essentially due to a quick photobleaching. In the near future, we aim to perfect the protocol of subcellular localization or, eventually, our compounds by enhancing their fluorescent capacity with simple chemical modifications. By continuing the investigation of subcellular transport and determining the biodistribution properties at the cellular level will help us to determine the mechanism of action of our Imiqualines. Quantitative assessment of the subcellular distribution of small molecules inside cells remains a challenge and we hope that progress in this field will continue to accelerate allowing us to obtain better results.

Acknowledgements We would like to thank Marjorie Damian from the team Cellular Pharmacology (IBMM, Montpellier, France) directed by Dr. Jean-Louis Banères for technical support to record UV and fluorescence spectra. We also thank Marie-Pierre Blanchard, head of the MRI Imaging Platform at the Functional Genomics Institute belonging to the Biocampus of Montpellier (France), for having recorded all the data relating to confocal microscopy.

References

1. Deleuze-Masquefa C, Moarbess G, Bonnet P-A, Pinguet F, Bazarbachi A, Bressolle F Imidazo[1,2-a]quinoxalines and derivatives thereof for treating cancers. WO/2009/043934, April 9, 2009
2. Moarbess G, Deleuze-Masquefa C, Bonnard V, Gayraud-Paniagua S, Vidal JR, Bressolle F, Pinguet F, Bonnet PA (2008) In vitro and in vivo anti-tumoral activities of imidazo[1,2-a]Quinoxaline, Imidazo[1,5-a]Quinoxaline, and Pyrazolo[1,5-a]Quinoxaline derivatives. Bioorg Med Chem 16(13):6601–6610. https://doi.org/10.1016/j.bmc.2008.05.022

3. Deleuze-Masquefa C, Moarbess G, Khier S, David N, Gayraud-Paniagua S, Bressolle F, Pinguet F, Bonnet PA (2009) New imidazo[1,2-a]quinoxaline Derivatives: synthesis and in vitro activity against human melanoma. Eur J Med Chem 44(9):3406–3411. https://doi.org/10.1016/j.ejmech.2009.02.007
4. Zghaib Z, Guichou J-F, Vappiani J, Bec N, Hadj-Kaddour K, Vincent L-A, Paniagua-Gayraud S, Larroque C, Moarbess G, Cuq P, Kassab I, Deleuze-Masquéfa C, Diab-Assaf M, Bonnet P-A (2016) New imidazoquinoxaline derivatives: synthesis, biological evaluation on melanoma, effect on tubulin polymerization and structure–activity relationships. Bioorg Med Chem 24(11):2433–2440. https://doi.org/10.1016/j.bmc.2016.04.004
5. Courbet A, Bec N, Constant C, Larroque C, Pugniere M, Messaoudi SE, Zghaib Z, Khier S, Deleuze-Masquefa C, Gattacceca F (2017) Imidazoquinoxaline anticancer derivatives and imiquimod interact with tubulin: characterization of molecular microtubule inhibiting mechanisms in correlation with cytotoxicity. PLoS One 12(8):e0182022. https://doi.org/10.1371/journal.pone.0182022
6. Nabbouh AI, Hleihel RS, Saliba JL, Karam MM, Hamie MH, Wu H-CJM, Berthier CP, Tawil NM, Bonnet P-AA, Deleuze-Masquefa C, Hajj, H (2017) A. E. Imidazoquinoxaline derivative EAPB0503: A promising drug targeting mutant nucleophosmin 1 in acute myeloid leukemia. Cancer 123(9):1662–1673. https://doi.org/10.1002/cncr.30515
7. Chouchou A, Patinote C, Cuq P, Bonnet P-A (2018) Deleuze-Masquéfa C Imidazo[1,2-a]quinoxalines derivatives grafted with amino acids: synthesis and evaluation on A375 melanoma cells. Mol Basel Switz 23 (11). https://doi.org/10.3390/molecules23112987
8. Patinote C, Bou Karroum N, Moarbess G, Deleuze-Masquefa C, Hadj-Kaddour K, Cuq P, Diab-Assaf M, Kassab I, Bonnet P-A (2017) Imidazo[1,2-a]Pyrazine, Imidazo[1,5-a]Quinoxaline and Pyrazolo[1,5-a]Quinoxaline derivatives as IKK1 and IKK2 inhibitors. Eur J Med Chem 138:909–919. https://doi.org/10.1016/j.ejmech.2017.07.021
9. Chouchou A, Marion B, Enjalbal C, Roques C, Cuq P, Bonnet P-A, Bressolle-Gomeni FMM, Deleuze-Masquéfa C (2018) Liquid chromatography-electrospray ionization-tandem mass spectrometry method for quantitative estimation of new imiqualine leads with potent anticancer activities in rat and mouse plasma. application to a pharmacokinetic study in mice. J Pharm Biomed Anal 148:369–379. https://doi.org/10.1016/j.jpba.2017.10.025
10. Karroum NB, Patinote C, Deleuze-Masquéfa C, Moarbess G, Diab-Assaf M, Cuq P, Kassab I, Bonnet P-A (2018) Methylation of imidazopyrazine, imidazoquinoxaline, and pyrazoloquinoxaline through Suzuki–Miyaura cross coupling. Chem Heterocycl Compd 54(2):183–187. https://doi.org/10.1007/s10593-018-2252-8
11. Deleuze-Masquefa C, Bonnet P-A, Cuq P, (2016) Patinote C New Imidazo[1,2-A]quinoxalines and derivates thereof for the treatment of cancer. WO/2016/107895, July 7, 2016
12. Gonçalves MST (2009) Fluorescent labeling of biomolecules with organic probes. Chem Rev 109(1):190–212. https://doi.org/10.1021/cr0783840
13. Specht EA, Braselmann E, Palmer AEA (2017) Critical comparative review of fluorescent tools for live-cell imaging. Annu Rev Physiol 79(1):93–117. https://doi.org/10.1146/annurev-physiol-022516-034055
14. Oliveira E, Bértolo E, Núñez C, Pilla V, Santos HM, Fernández-Lodeiro J, Fernández-Lodeiro A, Djafari J, Capelo JL, Lodeiro C (2017) Green and red fluorescent dyes for translational applications in imaging and sensing analytes: a dual-color. Flag ChemistryOpen 7(1):9–52. https://doi.org/10.1002/open.201700135
15. Rodriguez EA, Campbell RE, Lin JY, Lin MZ, Miyawaki A, Palmer AE, Shu X, Zhang J, Tsien RY (2017) The growing and glowing toolbox of fluorescent and photoactive proteins. Trends Biochem Sci 42(2):111–129. https://doi.org/10.1016/j.tibs.2016.09.010
16. Garland M, Yim JJ, Bogyo MA (2016) Bright future for precision medicine: advances in fluorescent chemical probe design and their clinical application. Cell Chem Biol 23(1):122–136. https://doi.org/10.1016/j.chembiol.2015.12.003
17. Liu H-W, Chen L, Xu C, Li Z, Zhang H, Zhang X-B, Tan W (2018) Recent progresses in small-molecule enzymatic fluorescent probes for cancer imaging. Chem Soc Rev 47(18):7140–7180. https://doi.org/10.1039/C7CS00862G
18. Qiu F, Wang D, Zhu Q, Zhu L, Tong G, Lu Y, Yan D, Zhu X (2014) Real-time monitoring of anticancer drug release with highly fluorescent star-conjugated copolymer as a drug carrier. Biomacromol 15(4):1355–1364. https://doi.org/10.1021/bm401891c
19. Sailer BL, Valdez JG, Steinkamp JA, Darzynkiewicz Z, Crissman HA (1997) Monitoring uptake of ellipticine and its fluorescence lifetime in relation to the cell cycle phase by flow cytometry. Exp Cell Res 236(1):259–267. https://doi.org/10.1006/excr.1997.3717
20. Jain S, Diwan A, Sardana S Development and validation of UV spectroscopy and RP-HPLC Methods for estimation of imiquimod. No. 04, 6
21. Zhao B, Rong Y-Z, Huang X-H, Shen J-S (2007) Experimental and theoretical study on the structure and electronic spectra of imiquimod and its synthetic intermediates. Bioorg Med Chem Lett 17(17):4942–4946. https://doi.org/10.1016/j.bmcl.2007.06.020
22. Patinote C, Hadj-Kaddour K, Damian M, Deleuze-Masquéfa C, Cuq P, Bonnet P-A (2017) Fluorescence study of imidazoquinoxalines. J Fluoresc 27(5):1607–1611. https://doi.org/10.1007/s10895-017-2097-z
23. Wilson K, Webster SP, Iredale JP, Zheng X, Homer NZ, Pham NT, Auer M, Mole DJ (2017) Detecting drug-target binding in cells using fluorescence-activated cell sorting coupled with mass spectrometry analysis. Methods Appl Fluoresc 6(1):015002. https://doi.org/10.1088/2050-6120/aa8c60
24. Marzagalli M, Moretti RM, Messi E, Marelli MM, Fontana F, Anastasia A, Bani MR, Beretta G, Limonta P (2018) Targeting melanoma stem cells with the vitamin E derivative δ-Tocotrienol. Sci Rep 8(1):1–13. https://doi.org/10.1038/s41598-017-19057-4
25. FluoroBrite DMEM, Media - FR https://www.thermofisher.com/fr/fr/home/life-science/cell-culture/mammalian-cell-culture/classical-media/fluorobrite-media.html. Accessed 26 Nov 2019